

The disk evaporation model for the spectral features of low-luminosity active galactic nuclei

Erlin Qiao¹, B. F. Liu¹, Francesca Panessa² and J. Y. Liu³

qiaoel@nao.cas.cn

ABSTRACT

Observations show that the accretion flows in low-luminosity active galactic nuclei (LLAGNs) probably have a two-component structure with an inner hot, optically thin, advection dominated accretion flow (ADAF) and an outer truncated cool, optically thick accretion disk. As shown by Taam et al. (2012), the truncation radius as a function of mass accretion rate is strongly affected by including the magnetic field within the framework of disk evaporation model, i.e., an increase of the magnetic field results in a smaller truncation radius of the accretion disk. In this work, we calculate the emergent spectrum of an inner ADAF + an outer truncated accretion disk around a supermassive black hole based on the prediction by Taam et al. (2012). It is found that an increase of the magnetic field from $\beta = 0.8$ to $\beta = 0.5$ (with magnetic pressure $p_m = B^2/8\pi = (1 - \beta)p_{\text{tot}}$, $p_{\text{tot}} = p_{\text{gas}} + p_m$) results in an increase of ~ 8.7 times of the luminosity from the truncated accretion disk, meanwhile results in the peak emission of the truncated accretion disk shifting towards a higher frequency by a factor of ~ 5 times. We found that the equipartition of gas pressure to magnetic pressure, i.e., $\beta = 0.5$, failed to explain the observed anti-correlation between $L_{2-10\text{keV}}/L_{\text{Edd}}$ and the bolometric correction $\kappa_{2-10\text{keV}}$ (with $\kappa_{2-10\text{keV}} = L_{\text{bol}}/L_{2-10\text{keV}}$). The emergent spectra for larger value $\beta = 0.8$ or $\beta = 0.95$ can well explain the observed $L_{2-10\text{keV}}/L_{\text{Edd}}-\kappa_{2-10\text{keV}}$ correlation. We argue that in the disk evaporation model, the electrons in the corona are assumed

¹National Astronomical Observatories, Chinese Academy of Sciences, Beijing 100012, China

²INAF - Istituto di Astrofisica e Planetologia Spaziali di Roma (IAPS), Via del Fosso del Cavaliere 100, 00133 Roma, Italy

³National Astronomical Observatories /Yunnan Observatory, Chinese Academy of Sciences, P.O. Box 110, Kunming 650011, P. R. China

to be heated only by a transfer of energy from the ions to electrons via Coulomb collisions, which is reasonable for the accretion with a lower mass accretion rate. Coulomb heating is the dominated heating mechanism for the electrons only if the magnetic field is strongly sub-equipartition, which is roughly consistent with observations.

Subject headings: accretion, accretion disks — Black hole physics — galaxies: active — X-rays: galaxies

1. Introduction

Active galactic nuclei (AGNs) are believed to be powered by accretion onto super-massive black holes, which are strong sources emitting from radio to X-rays. The luminous AGNs, mainly including radio quiet quasars and bright Seyfert galaxies, are believed to be powered dominantly by a geometrically thin, optically thick, accretion disk extending down to the innermost stable circular orbits (ISCO) of a black hole (Shakura & Sunyaev 1973; Shields 1978; Malkan & Sargent 1982; Kishimoto, Antouncci & Blaes 2005; Shang et al. 2005; Liu et al. 2012). Observations show that accretion flows in low-luminosity active galactic nuclei (LLAGNs) are very different. A two-component structure of the accretion flow with an inner hot, optically thin, advection dominated accretion flow (ADAF), an outer cool, optically thick truncated accretion disk, and a jet are supported by a number of observational evidence for LLAGNs (Ho 2008 and the references therein). The observational evidence for such a structure in LLAGNs comes mainly from the broadband emission from the radio to X-rays (Lasota et al. 1996; Quataert et al. 1999; Di Matteo et al. 2000, 2003; Yuan et al. 2009; Li et al. 2009). For example, by fitting the spectral energy distribution (SED) of NGC 1097, Nemmen et al. (2006) found that the optical and X-ray portion of the SED can be well fitted by an inner ADAF and an outer accretion disk truncated at 225 Schwarzschild radii, and the observed radio emission can be very well interpreted by the synchrotron emission of a relativistic jet modeled within the framework of the internal shock scenario (Yuan et al. 2005). The presence of a jet in LLAGNs has been clearly detected by the VLBI radio observations (Falcke et al. 2000; Nagar et al. 2001). Meanwhile, theoretically, because of the positive Bernoulli parameter of the hot ADAF, it is probably that the formation of the bipolar jets are driven by the ADAF (Narayan & Yi 1995b; Blandford & Begelman 1999; Meier et al. 2001; Yuan et al. 2012a, b).

The evidence for the presence of an inner ADAF in LLAGNs is inferred from the very low luminosity and the very lower radiative efficiency estimated from the available mass supply rate (Ho 2009). In terms of Eddington luminosity, LLAGNs often have $\lambda \lesssim 0.01$ contrary to

the luminous AGNs with $\lambda \gtrsim 0.01$ (with $\lambda = L_{\text{bol}}/L_{\text{Edd}}$, $L_{\text{Edd}} = 1.26 \times 10^{38} M/M_{\odot} \text{ erg s}^{-1}$) (Panessa et al. 2006). The observed anti-correlation between the hard X-ray index $\Gamma_{2-10\text{keV}}$ and λ implies that LLAGNs may be dominated by ADAF (Gu & Cao 2009; Younes et al. 2011, 2012). Xu (2011) collected a LLAGN sample composed of 49 sources including 28 local Seyfert galaxies and 21 low-ionization nuclear emission-line regions (LINERs) with optical/UV and X-ray observations. It is found that there is a strong anti-correlation between α_{ox} and Eddington ratio λ for the sources with $\lambda \lesssim 10^{-3}$, which supports that ADAF model is a very promising candidate in LLAGNs.

The evidence for the truncation of the accretion disk in LLAGNs is inferred from the lack of a ‘big blue bump’, instead of a ‘big red bump’ (Nemmen et al. 2012). The very weak or absent broad iron K_{α} line, which is attributed to X-ray fluorescence off of an optically thick accretion disk extending down to a few Schwarzschild radii of luminous AGNs, also supports that the accretion disk truncates at a larger radius ($\sim 100 - 1000$ Schwarzschild radii) off the black hole in LLAGNs (Nandra et al. 2007). Quataert et al. (1999) fitted the optical/UV spectrum of M81 with a mass accretion rate of 0.01 Eddington accretion rate and an accretion disk truncated at 100 Schwarzschild radii. A similar fit to the optical/UV spectrum of NGC 4579 yielded a higher mass accretion rate of 0.03 Eddington accretion rate, while the truncation radius of the accretion disk is still 100 Schwarzschild radii (Quataert et al. 1999). The relationship between the truncation radius and the mass accretion rate is still controversial. By fitting the SEDs of a population of LLAGNs, Yuan & Narayan (2004) found that the lower Eddington ratio $L_{\text{bol}}/L_{\text{Edd}}$ was associated with a larger truncation radius. By studying 33 PG quasars with Fe K_{α} emission line detected by the *XMM-Newton* survey, Inoue, Terashima & Ho (2007) found that the Fe K_{α} line systematically becomes narrow with decreasing $L_{\text{bol}}/L_{\text{Edd}}$, which probably means that the truncation radius of the accretion disk increases with decreasing mass accretion rate. It is interesting that the inverse correlation between the truncation radius of the accretion disk and the mass accretion rate is also found in the low/hard spectral state of black hole X-ray binaries (Cabanac et al. 2009).

The physical mechanism for determining the truncation of the accretion disk has been proposed by many authors (Honma 1996; Manmoto & Kato 2000; Lu et al. 2004; Spruit & Deufel 2002; Dullemond & Spruit 2005). One of the promising model among them is the disk evaporation model, which was first proposed by Meyer & Meyer-Hofmeister (1994) for dwarf novae, established for black holes by Meyer et al. (2000a, b) and modified by Liu et al. (2002), where the decoupling of ions and electrons and Compton cooling effect are taken into account. The disk evaporation model has been applied to explain the spectral state transition in stellar-mass black holes (e.g., Meyer-Hofmeister & Meyer 2005; Qiao & Liu 2009; Qian et al. 2007). The spectral features of an inner ADAF and an outer truncated accretion disk predicted by the disk evaporation model in stellar-mass black holes were investigated

by Qiao & Liu (2010, 2012). The first application of disk evaporation model to interpret the truncation of the accretion disk in LLAGNs was from Liu et al. (1999), in which a theoretical relation between the truncation radius and the mass accretion rate was given. Taam et al. (2012) generalized the disk evaporation model in black hole X-ray binaries by including the effect of a magnetic field in accretion disk to apply the model to the truncation of the accretion disk in a large number of LLAGNs. It is found that the truncation radius of the accretion disk can be very strongly affected by the magnetic parameters β , which is defined as $p_m = B^2/8\pi = (1 - \beta)p_{\text{tot}}$, (where $p_{\text{tot}} = p_{\text{gas}} + p_m$, p_{gas} is gas pressure and p_m is magnetic pressure), describing the strength of the magnetic field in the accretion flows. Taam et al. (2012) found that the inclusion of magnetic field results in a smaller truncation radius compared to the case without magnetic field.

In this work, based on the prediction by Taam et al. (2012) for the truncation of the accretion disk, the emergent spectrum of a two-component structure with an inner ADAF and an outer truncated accretion disk around a supermassive black hole is calculated. It is found that the disk evaporation model can roughly reproduce the observed anti-correlation between the hard X-ray index $\Gamma_{2-10\text{keV}}$ and the Eddington ratio λ in LLAGNs (e.g., Gu & Cao 2009). As shown by Taam et al. (2012), the truncation radius of the accretion disk is very sensitive to β , which consequently affects the emergent spectrum. Our calculations show that the equipartition of gas pressure to magnetic pressure, i.e., $\beta = 0.5$, failed to explain the observed anti-correlation between $L_{2-10\text{keV}}/L_{\text{Edd}}$ and the bolometric correction $\kappa_{2-10\text{keV}}$ (with $\kappa_{2-10\text{keV}} = L_{\text{bol}}/L_{2-10\text{keV}}$). The emergent spectra for larger value $\beta = 0.8$ or $\beta = 0.95$ can well explain the observed $L_{2-10\text{keV}}/L_{\text{Edd}}-\kappa_{2-10\text{keV}}$ correlation. It is argued that the sub-equipartition of the magnetic field is reasonable in the case with a low mass accretion. In section 2, we briefly introduce the disk evaporation model. The emergent spectra of disk evaporation model are presented in section 3. Some applications of the disk evaporation model to LLAGNs are presented in section 4. Section 5 is the conclusion.

2. The Model

2.1. Truncation of the accretion disk

We consider a hot corona above a geometrically thin standard disk around a central black hole. In the corona, viscous dissipation leads to ion heating, which is partially transferred to the electrons by means of Coulomb collisions. This energy is then conducted down into lower, cooler, and denser corona. If the density in this layer is sufficiently high, the conductive flux is radiated away. If the density is too low to efficiently radiate energy, cool matter is heated up and evaporation into the corona takes place. The mass evaporation goes on

until an equilibrium density is established. The gas evaporating into the corona still retains angular momentum and with the role of viscosity will differentially rotate around the central object. By friction the gas loses angular momentum and drifts inward, and thus continuously drains mass from the corona towards the central object. This is compensated by a steady mass evaporation flow from the underlying disk. The process is driven by the gravitational potential energy released by friction in the form of heat in the corona. Therefore, mass accretes to the central object partially through the corona (evaporated part) and partially through the disk (the left part of the supplying mass). Such a model for black holes was established by Meyer et al. (2000a, b). The inflow and outflow of mass, energy, and angular momentum between neighboring zones were included by Meyer-Hofmeister & Meyer (2003). The effect of the viscosity parameter α is investigated by (Qiao & Liu 2009), and the effect of the magnetic parameter β is studied by (Qian et al. 2007). The model we used here is based on Liu & Taam (2009), in which the structure of the corona and the evaporation features are determined by the equation of state, equation of continuity, and equations of momentum and energy. The calculations show that the evaporation rate increases with decreasing distance in the outer region of the accretion disk, reaching a maximum value and then dropping towards the central black hole. Taam et al. (2012) generalized the results of disk evaporation model for black hole X-ray binaries by including the effect of viscosity parameters α and magnetic parameter β in accretion disks around a supermassive black hole. The maximum evaporation rate and the corresponding radius from the black hole as functions of α and β are given as (Taam et al. 2012),

$$\dot{m}_{\max} \approx 0.38\alpha^{2.34}\beta^{-0.41}, \quad (1)$$

$$r_{\min} \approx 18.80\alpha^{-2.00}\beta^{4.97}, \quad (2)$$

where the evaporation rate is in units of Eddington accretion rate \dot{M}_{Edd} ($\dot{M}_{\text{Edd}} = 1.39 \times 10^{18} M/M_{\odot} \text{ g s}^{-1}$), and the radius is in units of Schwarzschild radius R_{S} ($R_{\text{S}} = 2.95 \times 10^5 M/M_{\odot} \text{ cm}$).

If the accretion rate is higher than the maximum evaporation rate, the evaporation can only make a fraction of the disk accretion flow go to the corona and the optically thick disk is never completely truncated by evaporation. However, if the mass supply rate is less than the maximum evaporation rate, the matter in the inner region of the disk will be fully evaporated to form a geometrically thick, optically thin accretion inner region, which is generally called advection-dominated accretion flow (ADAF). The truncation radius of the disk can be generalized as (Taam et al. 2012),

$$r_{\text{tr}} \approx 17.3\dot{m}^{-0.886}\alpha^{0.07}\beta^{4.61}, \quad (3)$$

where \dot{m} is the mass supply rate from the most outer region of the accretion disk. If α , β and \dot{m} are specified, we can self-consistently get a two-component structure of the accretion flow with an inner ADAF and an outer truncated accretion disk. It can be seen that from Equation (3), the truncation radius is very weakly dependent on α , but strongly dependent on β . It is argued that the effect of magnetic fields on evaporation rate is a competition between its tendency to increase the evaporation as a result of the energy balance and to decrease the evaporation as a result of the pressure balance. The additional pressure contributed by the magnetic fields results in a greater heating via the shear stress. This effect is similar to an increase viscosity parameter and leads to an increase of evaporation rate in the inner region with little effect in the outer region. In this paper, because we focus on the truncation of the accretion disk in the outer region, the additional pressure contribution suppresses the evaporation at all distances as a result of force balance. The effect of the magnetic field results in little change in the value of the maximal evaporation rate, but make the evaporate curve move systematically inward, which means the truncation radius will decrease for a given mass accretion rate. Meanwhile, we address that Equation (3) is a good fit only when the mass accretion rate is less than half of the maximum evaporation rate, i.e., $\dot{m} \lesssim (1/2)\dot{m}_{\max} = 0.19\alpha^{2.34}\beta^{-0.41} \approx 0.01$ (assuming a standard viscosity parameter $\alpha = 0.3$). When the mass accretion rate is close to the maximum evaporation rate, the truncation radius deviates from the power-law expression of Equation (3). In this case, the truncation radius will be determined by detailed numerical calculations (Taam et al. 2012).

2.2. The ADAF model

Inside the truncation radius, the accretion flows are in the form of advection dominated accretion flow (ADAF) or radiatively inefficient accretion flow (RIAF) from our disk-evaporation model (Rees et al. 1982; Narayan & Yi 1994; Narayan et al. 1998; Quataert 2001; Narayan & McClintock 2008, and the references therein). The self-similar solution of ADAF was first proposed by Narayan & Yi (1994, 1995b), with which the spectrum of transient sources A0620-00 and V404 Cyg with lower luminosity were well fitted (Narayan et al. 1996). Later, the global solution of ADAF are conducted by several authors (Narayan et al. 1997; Manmoto 1997, 2000; Yuan et al. 1999, 2000; Zhang et al. 2010). The applications of ADAF to interpret the broadband spectrum of supermassive black holes can be seen, e.g., in Yuan et al. (2003) for the Galactic center, and by Quataert et al. (1999) for the LLAGN M81 and NGC 4579 and so on. All of them show that the self-similar solution is a good approximation at a radius far enough from the ISCO. For simplicity, in this paper, the self-similar solution of ADAF is adopted (Narayan & Yi 1995a, b). The structure of an ADAF surrounding a black hole with mass M can be calculated if the parameters including

\dot{m} , α and β are specified.

3. Numerical result

We calculate the emergent spectra predicted by the disk evaporation model for a two-component structure composed of an inner ADAF and a truncated accretion disk around a supermassive black hole with mass M when the parameters including \dot{m} , α and β are specified. In the calculation, we fix central black hole mass at $M = 10^8 M_\odot$, assuming a viscosity parameter of $\alpha = 0.3$, as adopted by Taam et al. (2012) for the spectral fits to LLAGNs.

The emergent spectra with mass accretion rates for $\beta = 0.8$ are plotted in the left panel of Figure 1 for mass accretion rates $\dot{m} = 0.01, 0.005, 0.003, 0.001$. The black-solid line is the total emergent spectrum for $\dot{m} = 0.01$, and the black-dashed line is the emission from the accretion disk with a truncation radius $r_{\text{tr}} = 310$ predicted by Equation (3). The maximum effective temperature of the truncated accretion disk is $\sim 2599\text{K}$, which has a typical emission peaking at $\sim 1.1\mu\text{m}$ (in L_ν vs. ν). The hard X-ray emission between 2-10 keV for $\dot{m} = 0.01$ can be described by a power law with a hard X-ray index $\Gamma = 1.65$, which is produced by the self-Compton scattering of the synchrotron and bremsstrahlung photons of the ADAF itself. With a decrease of the mass accretion rate to $\dot{m} = 0.005$, the predicted truncation radius of the accretion disk is $r_{\text{tr}} = 573$, which has a maximum effective temperature $\sim 1388\text{K}$ with a peak emission at $\sim 2.1\mu\text{m}$. Meanwhile, the hard X-ray index between 2-10 keV is $\Gamma = 1.75$. The blue-solid line in the left panel of Figure 1 is the total emergent spectrum for $\dot{m} = 0.005$, and the blue-dashed line is the emission from the truncated accretion disk. With a further decrease of the mass accretion rates to $\dot{m} = 0.003$ and $\dot{m} = 0.001$, the truncation radii of the accretion disk are $r_{\text{tr}} = 901$ and $r_{\text{tr}} = 2386$, which correspond to an effective temperature of the accretion disk of $\sim 874\text{K}$ and $\sim 321\text{K}$ with peak emissions at $\sim 3.3\mu\text{m}$ and $\sim 9\mu\text{m}$ respectively. Meanwhile, the hard X-ray indices are $\Gamma = 1.81$ for $\dot{m} = 0.003$ and $\Gamma = 1.98$ for $\dot{m} = 0.001$ respectively. The purple-solid line and the red-solid line in Figure 1 are the total emergent spectra for $\dot{m} = 0.003$ and $\dot{m} = 0.001$, and the purple-dashed and the red-dashed lines are the emissions from the truncated accretion disks respectively.

We plot the hard X-ray index $\Gamma_{2-10\text{keV}}$ as a function of Eddington ratio $L_{\text{bol}}/L_{\text{Edd}}$ for $\beta = 0.8$ in Figure 2 with a red line. Here the bolometric luminosity L_{bol} is calculated by integrating the emergent spectrum. It is found that there is an anti-correlation between $\Gamma_{2-10\text{keV}}$ and $L_{\text{bol}}/L_{\text{Edd}}$, which is qualitatively consistent with the observations in LLAGNs (Constantin et al. 2009; Wu & Gu 2009; Younes et al. 2011, 2012; Xu 2011). This is because, with the decrease of the mass accretion rate, the electron temperature of ADAF

T_e changes only slightly, and it is always around 10^9K (Mehadevan 1997). However, the decrease of the mass accretion rate will result in a direct decrease of the Compton scattering optical depth τ_{es} . So the Compton parameter $y = 4kT_e/m_e c^2 \text{Max}(\tau_{\text{es}}, \tau_{\text{es}}^2)$ of the ADAF decreases with decreasing mass accretion rate, consequently resulting in a softer spectrum, as also discovered in the low/hard spectral state of black hole X-ray binaries (Qiao & Liu 2010; 2013; Wu & Cao 2008; Yuan et al. 2005).

The emergent spectra with mass accretion rates for $\beta = 0.5$ are plotted in the right panel of Figure 1 for mass accretion rates $\dot{m} = 0.01, 0.005, 0.003, 0.001$. The black-solid line is the emergent spectrum for $\dot{m} = 0.01$, and the black-dashed line is the emission from the accretion disk with a truncation radius $r_{\text{tr}} = 30$ predicted by Equation 3. The maximum effective temperature of the truncated accretion disk is $\sim 1.4 \times 10^4\text{K}$, which has a typical UV emission peaking at $\sim 2075\text{\AA}$. The hard X-ray emission for $\dot{m} = 0.01$ in 2-10 keV can be described by a power law with a hard X-ray index $\Gamma = 1.78$. For $\dot{m} = 0.005, 0.003, 0.001$, the truncation radii of the accretion disk are $r_{\text{tr}} = 55.4, 87, 231$ respectively. The maximum effective temperature of the truncated accretion disk is $\sim 7635\text{K}, \sim 4862\text{K}$ and $\sim 1814\text{K}$ respectively, with the emission peaking at $3798\text{\AA}, 5964\text{\AA}$ and $1.6\mu\text{m}$ respectively. The hard X-ray indices between 2-10 keV are $\Gamma_{2-10\text{keV}} = 1.79, 1.85, 2.04$ respectively. We plot $\Gamma_{2-10\text{keV}}$ as a function of $L_{\text{bol}}/L_{\text{Edd}}$ for $\beta = 0.5$ in Figure 2 with the black line. It is also clear that there is an anti-correlation between $\Gamma_{2-10\text{keV}}$ and $L_{\text{bol}}/L_{\text{Edd}}$.

In order to clearly show the effect of the magnetic parameter β on the spectra, we fix the central black hole mass at $M = 10^8 M_{\odot}$, $\alpha = 0.3$ and $\dot{m} = 0.01$ to calculate the emergent spectra for $\beta = 0.8$ and $\beta = 0.5$. The emergent spectrum for $\beta = 0.8$ is plotted in Figure 3 with a red-solid line, and the emergent spectrum for $\beta = 0.5$ is plotted in Figure 3 with a black-solid line. The dashed lines are the emissions from the truncated accretion disk. The bolometric luminosity for $\beta = 0.8$ is $L_{\text{bol}} = 9.6 \times 10^{42} \text{ erg s}^{-1}$, which corresponds to $7.6 \times 10^{-4} L_{\text{Edd}}$. The radiative efficiency η (defined as $\eta = L_{\text{bol}}/\dot{M}c^2$) of the accretion flow for $\beta = 0.8$ is $\eta = 7.7 \times 10^{-3}$, which is much lower than the radiative efficiency $\eta \approx 0.1$ predicted by the standard accretion disk extending down to the ISCO of a non-rotating black hole. The bolometric luminosity for $\beta = 0.5$ is $L_{\text{bol}} = 3.1 \times 10^{43} \text{ erg s}^{-1}$, which corresponds to $2.5 \times 10^{-3} L_{\text{Edd}}$. The radiative efficiency of the accretion flow for $\beta = 0.5$ is $\eta = 0.025$. For comparison, we also plot the emergent spectrum for $\dot{m} = 0.01$ with the standard accretion disk extending down to the ISCO of a non-rotating black hole (the blue-solid line in Figure 3). The maximum temperature of the accretion disk is $\sim 4.2 \times 10^4\text{K}$, which has a emission peaking at $\sim 870.5\text{\AA}$ compared to the peak emission at $\sim 2075\text{\AA}$ for $\beta = 0.5$ and at $\sim 1.1\mu\text{m}$ for $\beta = 0.8$.

It has been demonstrated that the emergent spectra predicted by the disk evaporation

model can be strongly affected by the magnetic parameter β . The effect of β to the emergent spectrum is mainly from the emission of the truncated accretion disk. From Equation (3), an increase of β from 0.5 to 0.8 will result in a $(0.8/0.5)^{4.61} \approx 8.7$ times increase of the truncation radius of the accretion disk. Because the luminosity of the truncated accretion disk $L_{\text{disk}} \propto r_{\text{tr}}^{-1}$, the truncated accretion disk luminosity will decrease by a factor of 8.7. Meanwhile, because the maximum effective temperature of the truncated accretion disk $T_{\text{eff,max}} \propto r_{\text{tr}}^{-3/4}$, an increase of β from 0.5 to 0.8 will result in the peak emission of the truncated accretion disk shifting towards a lower frequency by a factor of ~ 5 times, e.g., taking $M = 10^8 M_{\odot}$, assuming viscosity parameter $\alpha = 0.3$, for $\dot{m} = 0.01$, the peak emission of the truncated accretion disk is at $\sim 2075 \text{\AA}$ for $\beta = 0.5$ and at $\sim 1.1 \mu m$ for $\beta = 0.8$. For the inner ADAF, a change of β mainly affects the radio emission, while it has only very little effect on the optical/UV and X-ray emission. The luminosity of ADAF $L_{\text{ADAF}} \propto \beta$, so a change of β from 0.5 to 0.8 will also imply a little change in the luminosity of the ADAF (Taam et al. 2012; Mahadevan 1997).

In order to show the effect of the black hole mass on the emergent spectra, we plot the emergent spectra for different black hole masses as comparisons. The emergent spectra for $M = 10^6 M_{\odot}$ with mass accretion rates $\dot{m} = 0.01, 0.005, 0.003, 0.001$ are plotted in Figure 4 for the left panel with $\beta = 0.8$, and for the right panel with $\beta = 0.5$. The emergent spectra for $M = 10^9 M_{\odot}$ with mass accretion rates $\dot{m} = 0.01, 0.005, 0.003, 0.001$ are plotted in Figure 5 for the left panel with $\beta = 0.8$, and for the right panel with $\beta = 0.5$.

4. Comparison with observations—Bolometric Correction $\kappa_{2-10\text{keV}}$

Generally, the bolometric luminosity of AGNs is estimated by multiplying a suitable bolometric correction at a given band. So far the most secure measurements to the bolometric luminosity is from X-ray observations. The X-ray bolometric correction $\kappa_{2-10\text{keV}}$ is determined from the mean energy distribution calculated from 47 luminous, mostly luminous quasars (Elvis et al. 1994), in which $\kappa_{2-10\text{keV}} \approx 30$. However, since the SED of AGNs can change much with mass accretion rate, it is not a good approximation to correct the bolometric luminosity with a single correction factor. A correlation between $\kappa_{2-10\text{keV}}$ and Eddington ratio λ is found by Vasudevan & Fabian (2007; 2009), in which $\kappa_{2-10\text{keV}}$ is calculated for a sample with simultaneous X-ray/Optical-UV observations. It is found that $\kappa_{2-10\text{keV}} \approx 15 - 30$ for $\lambda \lesssim 0.1$, $\kappa_{2-10\text{keV}} \approx 20 - 70$ for $0.1 \lesssim \lambda \lesssim 0.2$, and $\kappa_{2-10\text{keV}} \approx 70 - 150$ for $\lambda \gtrsim 0.2$ respectively. By compiling the SEDs of a small LLAGN sample, Ho (1999b) found that the median bolometric correction is $\kappa_{2-10\text{keV}} \approx 8$. A more extensive data set suggested a value larger by a factor of 2 (Ho 2000; 2009), having a median value $\kappa_{2-10\text{keV}} \approx 15.8$.

Because LLAGNs tend to be "X-ray-loud", they have smaller values of $\kappa_{2-10\text{keV}}$ compared with the luminous sources. This is consistent with the results of vasudevan & Fabian (2007; 2009) and Elvis et al. (1994).

We collect a sample composed of 10 LLAGNs, including NGC 1097, NGC 3031, NGC 4203, NGC 4261, NGC 4374, NGC 4450, NGC 4486, NGC 4579, NGC 4594 and NGC 6251 with 2-10 keV luminosity $L_{2-10\text{keV}}$ measurement and bolometric luminosity measurement from Ho (2009). The bolometric luminosity is obtained by integrating the interpolated SEDs shown in Ho (1999b) and Ho et al. (2000). The black hole masses are also collected by Ho (1999b) and Ho (2000). The bolometric correction $\kappa_{2-10\text{keV}}$ as a function of $L_{2-10\text{keV}}/L_{\text{Edd}}$ is plotted with the sign \diamond in Figure 6. Ho (2009) conservatively estimated that the errors of $L_{\text{bol}}/L_{2-10\text{keV}}$ of the sources in the sample should be within 0.3 dex. The best-fitting linear regression for the correlation between $\kappa_{2-10\text{keV}}$ and $L_{2-10\text{keV}}/L_{\text{Edd}}$ is as follows:

$$\kappa_{2-10\text{keV}} = -4.8 - 3.0 \times \log_{10}(L_{2-10\text{keV}}/L_{\text{Edd}}), \quad (4)$$

plotted as a dotted-line in Figure 6.

In order to compare with observations, we calculate the emergent spectra predicted by the disk evaporation model. As shown in section 3.1, magnetic parameter β has significant effects on the emergent spectrum, we calculate the emergent spectra for $\beta = 0.8$, $\beta = 0.95$, and $\beta = 0.5$ for comparisons. By integrating the emergent spectrum, we calculate the 2-10 keV luminosity $L_{2-10\text{keV}}$ and the bolometric luminosity L_{bol} , with which we can calculate $\kappa_{2-10\text{keV}}$ and $L_{2-10\text{keV}}/L_{\text{Edd}}$.

Fixing $\beta = 0.8$, taking $M = 10^8 M_{\odot}$ and assuming $\alpha = 0.3$, the ratio of 2-10keV luminosity $L_{2-10\text{keV}}$ to Eddington luminosity L_{Edd} is $L_{2-10\text{keV}}/L_{\text{Edd}} = 8.45 \times 10^{-5}$, 1.40×10^{-5} , 4.13×10^{-6} , 2.90×10^{-7} , and the bolometric correction is $\kappa_{2-10\text{keV}} = 9.0, 12.2, 14.2, 22.6$ for $\dot{m} = 0.01, 0.005, 0.003, 0.001$ respectively. $\kappa_{2-10\text{keV}}$ as a function of $L_{2-10\text{keV}}/L_{\text{Edd}}$ is plotted with a red-solid line in Figure 6. It can be seen that there is an anti-correlation between $L_{2-10\text{keV}}/L_{\text{Edd}}$ and $\kappa_{2-10\text{keV}}$. In order to check the effect of the black hole mass on $L_{2-10\text{keV}}/L_{\text{bol}} - \kappa_{2-10\text{keV}}$ correlation, we take different black hole masses for comparisons. For $M = 10^6 M_{\odot}$, $\kappa_{2-10\text{keV}}$ as a function of $L_{2-10\text{keV}}/L_{\text{bol}}$ is plotted with a black-solid line in Figure 6. For $M = 10^9 M_{\odot}$, $\kappa_{2-10\text{keV}}$ as a function of $L_{2-10\text{keV}}/L_{\text{bol}}$ is plotted with a blue-solid line in Figure 6. It can be seen that the effect of the black hole mass on $L_{2-10\text{keV}}/L_{\text{Edd}} - \kappa_{2-10\text{keV}}$ correlation is very weak. As an extreme example, we also plot $L_{2-10\text{keV}}/L_{\text{Edd}} - \kappa_{2-10\text{keV}}$ correlation for $\beta = 0.95$ in Figure 6. The red long-dashed, black long-dashed, blue long-dashed lines are for $M = 10^8 M_{\odot}$, $M = 10^6 M_{\odot}$ and $M = 10^9 M_{\odot}$ respectively.

Fixing $\beta = 0.5$, taking $M = 10^8 M_{\odot}$ and assuming $\alpha = 0.3$, the ratio of 2-10keV luminosity $L_{2-10\text{keV}}$ to Eddington luminosity L_{Edd} is $L_{2-10\text{keV}}/L_{\text{Edd}} = 8.94 \times 10^{-5}$, 1.87×10^{-5} ,

5.32×10^{-6} , 3.04×10^{-7} , and the bolometric correction is $\kappa_{2-10\text{keV}} = 27.5, 37.5, 50.3, 112.6$ respectively. $\kappa_{2-10\text{keV}}$ as a function of $L_{2-10\text{keV}}/L_{\text{Edd}}$ is plotted with a red short-dashed line in Figure 6. The bolometric correction $\kappa_{2-10\text{keV}}$ as a function of $L_{2-10\text{keV}}/L_{\text{Edd}}$ for $M = 10^6 M_{\odot}$ is plotted with a black short-dashed line in Figure 6, and for $M = 10^9 M_{\odot}$ is plotted with a blue short-dashed line in Figure 6.

From Figure 6, it is clear that the bolometric correction strongly depends on β . $L_{2-10\text{keV}}/L_{\text{bol}} - \kappa_{2-10\text{keV}}$ correlation predicted by $\beta = 0.8$ or $\beta = 0.95$ can well explain the observations, while the prediction by $\beta = 0.5$ severely deviates from the observations. Although our model for larger β can roughly interpret the $L_{2-10\text{keV}}/L_{\text{bol}} - \kappa_{2-10\text{keV}}$ correlation, it is still a few sources lay below the model line. This may be because, in this work, for simplicity, we assume that, outside the truncation radius, the accretion flow exists in the form of a pure standard accretion disk. However, according to the disk evaporation model, outside the truncation radius, the matter should be in the form of "disk+corona", but not the pure stand accretion disk. The emission from the corona will result in an increase of the X-ray emission, which will make the bolometric correction decrease. Consequently, the model-predicted $\kappa_{2-10\text{keV}}$ will systematically shift downward. We also need to keep in mind that, due to the inner ADAF dominating the X-ray emission, the emission contribution from the outer corona to the bolometric correction will be very small, so still the data support a bigger value of $\beta = 0.8$ or $\beta = 0.95$.

Theoretically, it would be useful to understand how the magnetic parameter is determined and how it is constrained. The value of β can be approximately known from the numerical simulations (e.g., Balbus & Hawley 1998). Detailed MHD numerical simulations for the formation of a magnetized corona have shown that a strongly magnetized corona can form above an initially weakly magnetized disk (e.g., Miller & Stone 2000; Machida et al. 2000; Hawley & Balbus 2002). However, in the disk evaporation model, we consider a slab corona in a large vertical extent, in which the corona is vertically stratified, in contrast to an isothermal torus as from MHD simulations. Furthermore, thermal conduction in vertical direction is taken into account, which will make an efficient mass evaporation from the disk to the corona, resulting in a higher mass density than in the coronal envelope seen in MHD simulations. More importantly, in the disk evaporation model, the electrons in the corona are assumed to be heated only by a transfer of energy from the ions to electrons via Coulomb collisions, which is reasonable for the accretion with a lower mass accretion rate (Narayan 1995b). Coulomb heating is the dominated heating mechanism for the electrons only if the magnetic field is strongly sub-equipartition (i.e., ratio of gas pressure to magnetic pressure > 10) (Malzac & Belmont 2009). The spectral modeling of Sgr A* showed that an additional direct heating to electrons is required, which is probably produced by magnetohydrodynamics turbulence, magnetic reconnection and weak shocks (Yuan et al. 2003). However, the

magnetic heating mechanism to the electrons is very unclear, consequently still a weak magnetic field, i.e., a high value of β is assured in the case of a lower mass accretion rate within the framework of disk evaporation model.

5. Conclusion

Based on the prediction by Taam et al. (2012) of a truncation radius of the accretion disk on the mass accretion rate by including the magnetic field, we have calculated the emergent spectrum of an inner ADAF + an outer truncated accretion disk around a super-massive black hole. It is found that the disk evaporation model can roughly reproduce the observed anti-correlation between hard X-ray index $\Gamma_{2-10\text{keV}}$ and Eddington ratio λ for $\lambda \lesssim 10^{-3}$ in LLAGNs. As shown by Taam et al. (2012), the truncation radius of the accretion disk is sensitive to the magnetic parameter β , which consequently affects the emergent spectrum. Our calculations show that the equipartition of gas pressure to magnetic pressure, i.e., $\beta = 0.5$, failed to explain the observed anti-correlation between $L_{2-10\text{keV}}/L_{\text{Edd}}$ and the bolometric correction $\kappa_{2-10\text{keV}}$. The resulted spectra for larger value $\beta = 0.8$ or $\beta = 0.95$ can better explain the observed $L_{2-10\text{keV}}/L_{\text{Edd}}-\kappa_{2-10\text{keV}}$ correlation. It is argued that in the disk evaporation model, the electrons in the corona are assumed to be heated only by a transfer of energy from the ions to electrons via Coulomb collisions, which is reasonable for the accretion with a lower mass accretion rate. Coulomb heating is the dominated heating mechanism for the electrons only if the magnetic field is strongly sub-equipartition, which is roughly consistent with observations.

We thank the very useful discussions with Prof. R. E. Taam from Northwestern University. This work is supported by the National Natural Science Foundation of China (grants 11033007 and 11173029), by the National Basic Research Program of China-973 Program 2009CB824800.

REFERENCES

- Blandford, Roger D., & Begelman, Mitchell C. 1999, MNRAS, 303, 1
- Cabanac, C., Fender, R. P., Dunn, R. J. H., & Kording, E. G. 2009, MNRAS, 396, 1415
- Di Matteo, T., Quataert, E., Allen, S. W., et al. 2000, MNRAS, 311,507
- Di Matteo, T., Allen, S. W., Fabian, A. C., Wilson, A. S., & Young, A. J. 2003, ApJ, 582,

- Dullemond, C. R., & Spruit, H. C. 2005, *A&A*, 434, 415
- Elvis, M., Wilkes, Belinda J., McDowell, Jonathan C., Green, Richard F., & Bechtold, J. 1994, *ApJS*, 95, 1
- Falcke, H., Nagar, Neil M., Wilson, Andrew S., & Ulvestad, James S. 2000, *A&A*, 542, 197
- Falcke, Heino, Nagar, Neil M., Wilson, Andrew S., & Ulvestad, James S. 2000, *ApJ*, 542, 197
- Gu, M., & Cao, X. 2009, *MNRAS*, 399, 349
- Ho, Luis C. 1999b, *ApJ*, 516, 672
- Ho, Luis C. et al., 2000, *ApJ*, 541, 120
- Ho, Luis C. 2008, *ARA&A*, 46, 475
- Ho, Luis C. 2009, *ApJ*, 699, 626
- Honma, F. 1996, *PASJ*, 48, 77
- Inoue, Hirohiko, Terashima, Yuichi, & Ho, Luis C. 2007, *ApJ*, 662, 860
- Kishimoto, M., Antonucci, R., & Blaes, O., 2005, *MNRAS*, 364, 640
- Lasota, J.-P., Abramowicz, M. A., Chen, X., et al. 1996, *ApJ*, 462, 142
- Li, Y.-R., Yuan, Y.-F., Wang, J.-M., Wang, J.-C., & Zhang, S. 2009, *ApJ*, 699, 513
- Liu, B. F., Yuan, W., Meyer, F., Meyer-Hofmeister, E., & Xie, G. Z. 1999, *ApJL*, 527, 17
- Liu, B. F., Mineshige, S., Meyer, F., Meyer-Hofmeister, E., & Kawaguchi, T. 2002, *ApJ*, 575, 117
- Lu, J.-F., Lin, Y.-Q., & Gu, W.-M. 2004, *ApJ*, 602, L37
- Liu, J. Y., Liu, B. F., Qiao, E. L., & Mineshige, S. 2012, *ApJ*, 754, 81
- Malkan, M. A., & Sargent, W. L. W., 1982, *ApJ*, 254, 22
- Mahadevan, R. 1997, *ApJ*, 477, 585
- Manmoto, T., & Kato, S. 2000, *ApJ*, 538, 295
- Meier, David L., Koide, Shinji, & Uchida, Yutaka 2001, *Science*, 291, 84

- Meyer, F., Liu, B. F., & Meyer-Hofmeister, E. 2000a, *A&A*, 361, 175
- Meyer, F., Liu, B. F., & Meyer-Hofmeister, E. 2000b, *A&A*, 354, L67
- Meyer, F., Liu, B. F., & Meyer-Hofmeister, E. 2007, *A&A*, 463, 1
- Meyer, F., & Meyer-Hofmeister, E. 2002, *A&A*, 392, 5
- Meyer, F., & Meyer-Hofmeister, E. 1994, *A&A*, 288, 175
- Meyer-Hofmeister, E., & Meyer, F. 2001, *A&A*, 380, 739
- Nagar, Neil M., Wilson, Andrew S., & Falcke, Heino 2001, *ApJ*, 559, 87
- Nandra, K., O’Neill, P. M., George, I. M., & Reeves, J. N. 2007, *MNRAS*, 382, 194
- Narayan, R., Mahadevan, R., & Quataert, E. 1998, in *The Theory of Black Hole Accretion Discs*, ed. M. A. Abramowicz, G. Bjornsson, & J. E. Pringle (Cambridge: Cambridge Univ. Press), 148
- Narayan, R., & Yi, I. 1995a, *ApJ*, 444, 231
- Narayan, R., & Yi, I. 1995b, *ApJ*, 452, 710
- Nemmen, R. S., Storchi-Bergmann, T., Yuan, F., Eracleous, M., Terashima, Y. et al. 2006, *ApJ*, 643, 652
- Nemmen, R. S., Storchi-Bergmann, T., & Eracleous, M. 2012, *ApJ*, submitted (arXiv: 1112.4640)
- Panessa, F., Bassani, L., Cappi, M., Dadina, M., Barcons, X. et al. 2006, *A&A*, 455, 173
- Qian, L., Liu, B. F., & Wu, X.-B. 2007, *ApJ*, 668, 1145
- Qiao, E., & Liu, B. 2009, *PASJ*, 61, 403
- Qiao, E., & Liu, B. 2010, *PASJ*, 62, 661
- Qiao, E., & Liu, B. F. 2012, *ApJ*, 744, 145
- Qiao, E., & Liu, B. F. 2013, *ApJ*, 764, 2
- Quataert, E., Di Matteo, T., Narayan, R., & Ho, L. 1999, *ApJ*, 525, L89

- Quataert, E. 2001, in *Probing the Physics of Active Galactic Nuclei by Multiwavelength Monitoring*, ed. B. M. Peterson, R. S. Polidan, & R. W. Pogge (San Francisco, CA: ASP), 71
- Shakura, N. I., & Sunyaev, R. A. 1973, *A&A*, 24, 337
- Shang, Z. et al. 2005, *ApJ*, 619, 41
- Shields, G. A. 1978, *Nature*, 272, 706
- Spruit, H. C., & Deufel, B. 2002, *A&A*, 387, 918
- Storchi-Bergmann, T., Nemmen da Silva, R., Eracleous, M., Halpern, J. P., & Wilson, A. S. 2003, *ApJ*, 598, 956
- Taam, Ronald E., Liu, B. F., Yuan, W., & Qiao, E. 2012, *ApJ*, 759, 65
- Vasudevan, R. V., & Fabian, A. C. 2007, *MNRAS*, 381, 1235
- Vasudevan, R. V., & Fabian, A. C. 2009, *MNRAS*, 392, 1124
- Xu, Ya-Di 2011, *ApJ*, 739, 64
- Younes, G., Porquet, D., Sabra, B., & Reeves, J. N. 2011, *A&A*, 530, 149
- Younes, G., Porquet, D., Sabra, B., Reeves, J. N., & Grosso, N. 2012, *A&A*, 539, 104
- Yuan, F. 1999, *ApJ*, 521, 55
- Yuan, F., Peng, Q., Lu, J.-F., & Wang, J. 2000, *ApJ*, 537, 236
- Yuan, F., Quataert, Eliot, & Narayan, Ramesh 2003, *ApJ*, 598, 301
- Yuan, F., & Narayan, Ramesh 2004, *ApJ*, 612, 724
- Yuan, F., Cui, W., & Narayan, R. 2005, *ApJ*, 620, 905
- Yuan, F., Yu, Z., & Ho, L. C. 2009, *ApJ*, 703, 1034
- Yuan, F., Bu, Defu, & Wu, Maochun 2012a, *ApJ*, 761, 130
- Yuan, F., Wu, Maochun, & Bu, Defu 2012b, *ApJ*, 761, 129
- Zhang, H., Yuan, F., & Chaty, S. 2010, *ApJ*, 717, 929

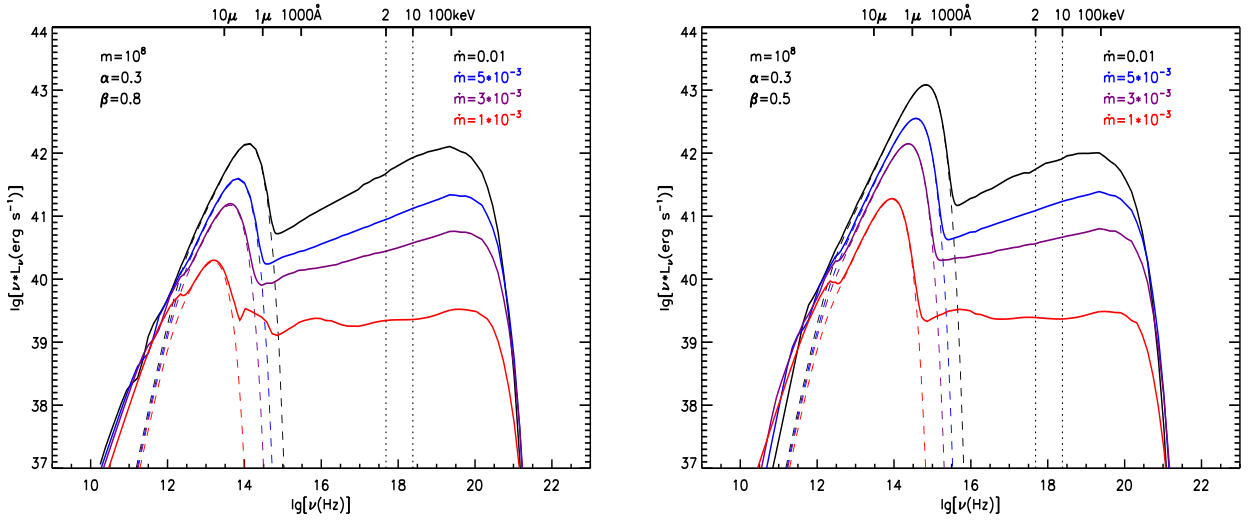


Fig. 1.—

Emergent spectra of an inner ADAF and an outer truncated accretion disk around a black hole predicted by the disk evaporation model with $M = 10^8 M_\odot$ assuming $\alpha = 0.3$. Left panel: $\beta = 0.8$ is adopted. From bottom to top, the solid lines are the combined emergent spectra from an inner ADAF plus an outer truncated accretion disk for $\dot{m} = 10^{-3}$, 3×10^{-3} , 5×10^{-3} and 0.01 respectively. The dashed line are the emergent spectra from the truncated accretion disk. Right panel: $\beta = 0.5$ is adopted, and the meaning of the line style is same with the left panel.

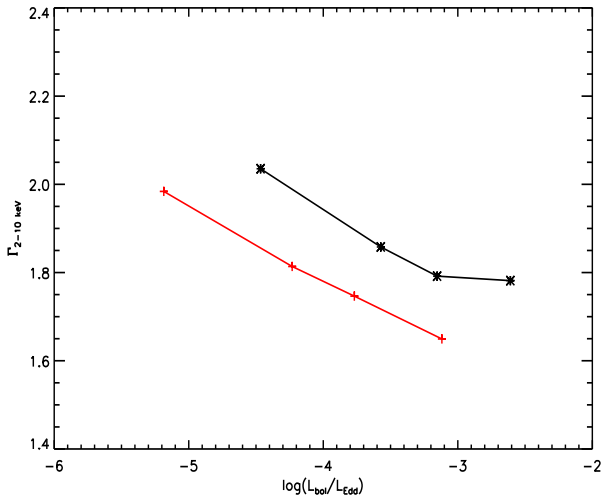


Fig. 2.—

Hard X-ray index $\Gamma_{2-10\text{keV}}$ as a function of Eddington ratio $L_{\text{bol}}/L_{\text{Edd}}$. In the calculations, we fix the black hole mass at $M = 10^8 M_{\odot}$, assuming a viscosity parameter $\alpha = 0.3$. The red line is for $\beta = 0.8$ and the black line is for $\beta = 0.5$.

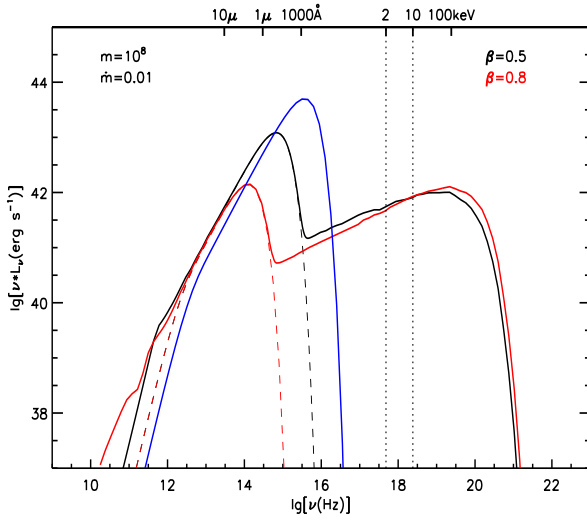


Fig. 3.—

Emergent spectra of an inner ADAF and an outer truncated accretion disk around a black hole predicted by the disk evaporation model with $M = 10^8 M_\odot$ assuming $\alpha = 0.3$. The solid-black line is for $\beta = 0.5$ and $\dot{m} = 0.01$, where the disk is truncated at $30R_S$. The red-solid line is for $\beta = 0.8$ and $\dot{m} = 0.01$, where the disk is truncated at $310R_S$. The dashed lines are the emergent spectra from the truncated accretion disk. The blue line is the emergent spectrum for $\dot{m} = 0.01$ with the standard accretion disk extending down to the ISCO of a non-rotating black hole.

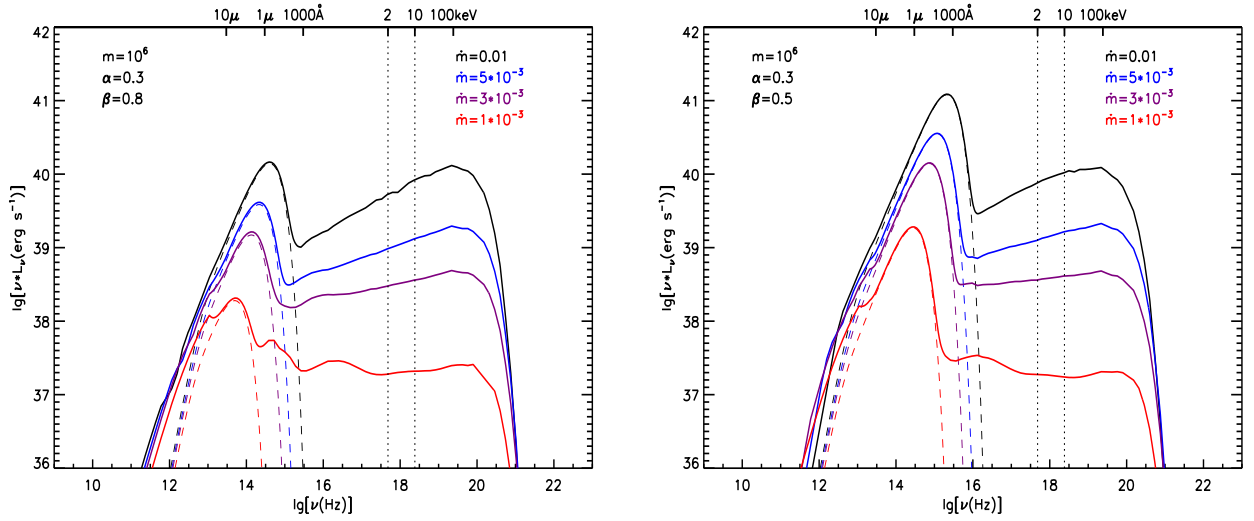


Fig. 4.—

Emergent spectra of an inner ADAF and an outer truncated accretion disk around a black hole predicted by the disk evaporation model with $M = 10^6 M_\odot$ assuming $\alpha = 0.3$. Left panel: $\beta = 0.8$ is adopted. From bottom to top, the solid lines are the combined emergent spectra from an inner ADAF plus an outer truncated accretion disk for $\dot{m} = 10^{-3}$, 3×10^{-3} , 5×10^{-3} and 0.01 respectively. The dashed lines are the emergent spectra from the truncated accretion disk. Right panel: $\beta = 0.5$ is adopted, and the meaning of the line style is same with the left panel.

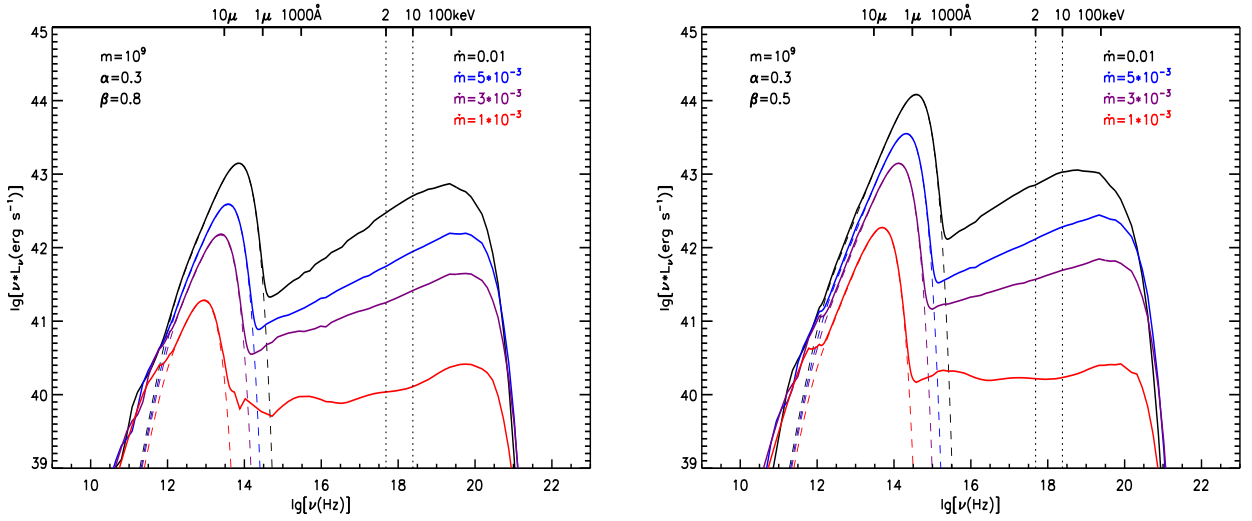


Fig. 5.—

Emergent spectra of an inner ADAF and an outer truncated accretion disk around a black hole predicted by the disk-evaporation model with $M = 10^9 M_\odot$ assuming $\alpha = 0.3$. Left panel: $\beta = 0.8$ is adopted. From bottom to top, the solid lines are the combined emergent spectra from an inner ADAF plus an outer truncated accretion disk for $\dot{m} = 10^{-3}$, 3×10^{-3} , 5×10^{-3} and 0.01 respectively. The dashed lines are the emergent spectra from the truncated accretion disk. Right panel: $\beta = 0.5$ is adopted, and the meaning of the line style is same with the left panel.

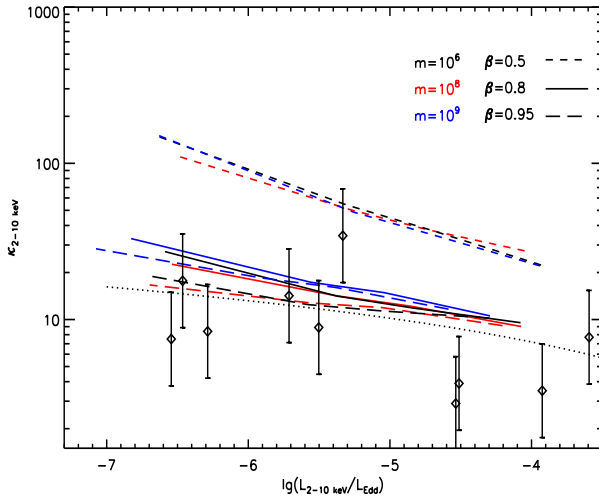


Fig. 6.—

Bolometric correction $\kappa_{2-10\text{keV}}$ as a function of $L_{2-10\text{keV}}/L_{\text{Edd}}$. The short-dashed line is for $\beta = 0.5$, the solid line is for $\beta = 0.8$ and the long-dashed line is for $\beta = 0.95$. The black line is for $M = 10^6 M_{\odot}$, red line is $M = 10^8 M_{\odot}$ and the blue line is for $M = 10^9 M_{\odot}$. In all the calculation, $\alpha = 0.3$ is adopted. The sign \diamond is the observed data, including NGC 1097, NGC 3031, NGC 4203, NGC 4261, NGC 4374, NGC 4450, NGC 4486, NGC 4579, NGC 4594 and NGC 6251 with 2-10 keV luminosity $L_{2-10\text{keV}}$ measurement and bolometric luminosity measurement from Ho (2009).